American Mineralogist, Volume 99, pages 2116–2125, 2014

What Lurks in the Martian Rocks and Soil? Investigations of Sulfates, Phosphates, and Perchlorates

Flower-like apatite recording microbial processes through deep geological time and its implication to the search for mineral records of life on Mars†

Si Sun[1], Lung S. Chan[1] and Yi-Liang Li[1,*]

[1]Department of Earth Sciences, The University of Hong Kong, Pokfulam Road, Hong Kong

Abstract

The biological cycling of phosphorus on Earth could be as early as the origin of life in early Archean. However, because of the low abundance and fine particle size, phosphate related to microbial ecophysiological activities in early sedimentary rocks, especially those deposited before the Great Oxidation Event (GOE, ca. 2.45–2.32 Ma), is still poorly addressed. It is not until recently that certain petrographic and mineralogical features of apatite in the early Precambrian sedimentary rocks were found related to microbial activities. In this study, we report high-resolution electron microscopic investigations on apatite from the Neoarchean to early Paleoproterozoic banded iron formations (BIFs), Mesoproterozoic to Lower Cambrian black shale and phosphorites, and Pliocene sediments. Apatite in BIFs occurs as 4–8 μm radial flowers with "petals" made of apatite rods. Their mineralogical and petrologic features are highly similar to those in the younger sedimentary rocks in which biomass have been confirmed to play an important role in the mineralization of phosphate. We suggest that these sedimentary rocks or sediments have experienced similar phosphogenetic processes mediated by biomass that led to the mineralization of phosphorus. The formation and preservation of phosphate (apatite) with conspicuous recognizable features in association with biological activities from Late Archean to Pliocene implies its universal significance in recording microbial processes through deep geological evolution. With mild dynamic processes, the martian (sub)surface has better preservation conditions than Earth, and the micro-structure of phosphate formed in environments mediated by microorganisms could be recognized by high-resolution observations on the surface of Mars or returned samples, if microbial life ever developed on Mars.

Keywords: Banded iron formations, phosphorite, phosphatization, deep time, life on Mars

Introduction

As early Mars could be habitable (e.g., Sleep 2010), martian life, if it ever existed, should be similar to microorganisms on Earth during early evolution (Rothschild 1990; Nisbet and Sleep 2001). The complicated mineral evolution on Earth with its co-evolving biosphere (Hazen et al. 2008, 2011) could be a reference to searching for evidence of life on Mars. Banded iron formations (BIF) that only deposited in the first half of life history on Earth (~3800 to 1800 Ma, with a short reappearance in Neoproterozoic era) bear records of intertwined evolution of Earth's early biosphere and geosphere. In view of rare corroborative microbial fossils (e.g., Schopf 1993, 2012; Brasier et al. 2002), controversial carbon isotopic records (Mojzsis et al. 1996; Van Zuilen et al. 2002; Lepland et al. 2002, 2005) and problematic lipid biomarkers in Archean sedimentary rocks (Brocks et al. 1999; Rasmussen et al. 2008; Brocks 2011), minerals in BIFs indicative of the existence of biological activities were considered as alternative proxies to trace the activity of early life on Earth (Li et al. 2011, 2013), and even life on Mars (e.g., Walter and Des Marais 1993; Horneck 2000).

Phosphorus (appearing as phosphate) is a common component in BIFs (e.g., Morris 1993; Bekker et al. 2010). Previous studies on phosphate in BIFs have focused on its petrology and geochemistry (e.g., Trendall and Blockley 1970; Morris 1973; Lepland et al. 2002, 2005; Nutman and Friend 2006). For example, Trendall and Blockley (1970) reported that the concentration of phosphorus in BIF from Dales Gorge was much higher than that in the rest of BIFs in Hamersley (0.03–0.16%), Western Australia; Morris (1973) and Pecoits et al. (2009) found phosphate in the Dales Gorge BIF occurring as semi-continuous layers or grains of ~10–120 μm under optical microscopes. However, the mineralogical habits of phosphate in BIFs, especially those related to biological activities, are still poorly understood due to its very low abundance and fine particle size (Li et al. 2011).

The ecosystems before the Great Oxidation Event (GOE, 2450–2320 Ma) were dominated by unicellular anaerobes of much lower primary productivities than those in the modern ocean (e.g., Bjerrum and Canfield 2002). Phosphatization of those unicellular organisms was not as significant as that of animal tissues or other multi-cellular life-forms that did not emerge until the Neoproterozoic era (Cook and Shergold 1984; Schulz and Schulz 2005; Bailey et al. 2007; Yin et al. 2007; Xiao and Schiffbauer 2008). With the advant of Ediacarian biota at ca. 635–542 Ma and the Cambrian Explosion at ca. 530–520 Ma,

* E-mail: yiliang@hku.hk

† Open access: Article available to all readers online. Special collection papers can be found on GSW at http://ammin.geoscienceworld.org/site/misc/specialissuelist.xhtml.

0003-004X/14/0010–2116$05.00/DOI: http://dx.doi.org/10.2138/am-2014-4794

Earth's biosphere entered an era with an unprecedented flourish of multi-cellular organisms and early animals (e.g., Bowring et al. 1993). Decayed animal tissues (e.g., Xiao et al. 1998; Zhang et al. 1998; Xiao and Knoll 2000; Yin et al. 2007), as well as other multi-cellular biomass (e.g., Schulz and Schulz 2005; Bailey et al. 2007) in the further oxidized geochemical environments (Canfield et al. 2007), favored the mineralization of phosphate and led to large-scale phosphorite deposits. Phosphates in these phosphorites with special structures and morphologies in association with microbial activities could thus be considered as a model for a better understanding of microbial phosphatization prior to GOE. Li et al. (2013) reported micrometer-sized flower-like apatite from both BIFs and Lower Cambrian phosphorite, and suggested that those apatite flowers with high similarities experienced similar biologically mediated phosphatization processes. However, more observations are needed to substantiate this hypothesis. In this study, we report similar apatite nanocrystals and micrometer-scale flower structures from 11 samples aged from 2728 to 3.6 Ma (Fig. 1; Table 1) to support that flower-like apatite in BIFs were precipitated with microbial mediation. Furthermore, the preservation of these apatite structures through such a deep geological time suggests that phosphates with similar structures could also be well preserved in martian sedimentary rocks, if life ever existed on Mars.

Samples

Pliocene sediment (3.6 Ma)

This sample was collected from the lower part of Kunlun Formation, Kunlun Pass area of northern Tibetan Plateau, China. With a magnetostratigraphic age of ~3.6 Ma (Song et al. 2005), the sediments deposited in a basin with extreme climatic and topographic conditions, such as desert, cold meadow, or steppe environments (Wang et al. 2008), and have not yet been subjected to lithification or metamorphism. Abundant animal fossils, such as fishes and gastropods, were identified in Kunlun Pass sediments (e.g., Wang et al. 2008).

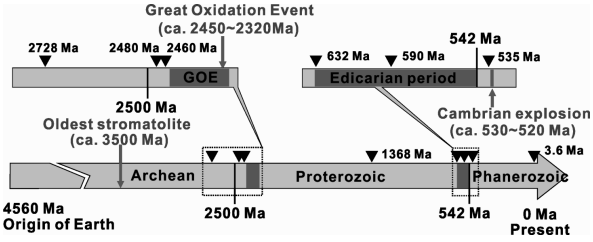

Figure 1. Studied samples (marked by triangles) on the timeline of Earth.

Table 1. Summary of mineralogical features of the apatite flowers from the Neoarchean to Pliocene geological records

Samples	Age (Ma)	Flower features	Grain features		Deposition environment	Postdepositional history	Evidence of biological activities
			In flower centers	Out of flowers			
Pliocene sediment (Kunlun Pass sediments)	3.6	–	–	60 ± 35 nm (length) 35 ± 10 nm (width); rounded to elliptic	–	None disgenesis or metamorphisms	Abundant fossils, such as fishes and gastropos, were identified (e.g., Wang et al. 2006)
Niutitang cherty phosphorite	535	–	–	150 ± 30 nm in diameter; polyhedron-like	continental shelf margin with deep water and low-tidal energy	Disgenesis	Abundant fossils, such as acritarch, algae, sponge and small animals, were identified (e.g., Steiner et al. 2005; Zhang et al. 2008)
Niutitang phosphate nodule	535	4–20 μm, with "petals" of porous apatite rods, which were coated by apatite thin apatite films	100–300 nm; rounded, elliptic or polyhedron	100–300 nm; rounded, elliptic to polyhedron-like	submarine discontinuity surfaces in hemipelagic environments	Disgenesis	Abundant fossils were examined in the hosting black shale (Steiner et al. 2001); alternating microlayers of organics and fabric phosphate, which was interpreted as phosphate replacement of originally calcified organisms
Niutitang phosphorite[a]	535	3–8 μm, with "petals" have porous structures and rough surfaces	100–200 nm in diameter	100–300 nm; polyhedron-like	redox interface of upwelling zone (Li et al. 2013)	Disgenesis	1. Abundant fossils, such as acritarch, algae, sponge and small animals, were identified (e.g., Steiner et al. 2005; Zhang et al. 2008) 2. Fossil moleculars of cyanobacteria were detected both by GC-MS and laser Raman spectroscope (Li et al. 2013)

(Continued on next page)

Neoproterozoic to Lower Cambrian phosphorite, phosphate and chert nodules (632–535 Ma)

Neoproterozoic to early Cambrian is an important interval in which Earth experienced the amalgamation and breakup of Rodinia supercontinent (e.g., Hoffman 1992; Unrug 1997), the subsequent climate disaster of Snowball Earth (e.g., Hoffman et al. 1998) and the flourish of multi-cellular organisms (Butterfield 2007). These processes collectively led to the deposition of large-scale phosphorite deposits with economic importance (Papineau 2010). Six samples collected from phosphorite or related sedimentary rocks deposited in this period were used in this study (Fig. 1; Table 1).

Three samples (one cherty phosphorite, one phosphate nodule embedded in black shale, and one phosphorite thin layer imbedded in black shale) are from Niutitang Formation, Guizhou province of southwestern China, which unconformably overlies Dengying Formation and is overlain by Mingxinshi Formation. The Niutitang Formation has an age of ~535 Ma determined by Re-Os isochron method (Jiang et al. 2007), and bears abundant fossils of acritarch, algae, sponge, and small animals (e.g., Steiner et al. 2005; Zhang et al. 2008). The Niutitang Biota is slightly older than the well-known Chengjiang Fauna (525 Ma, Hou et al. 2004). The fourth sample is from the Neoproterozoic phosphorite deposit intercalated with carbonate layers from the upper sequence of Doushantuo Formation in Kaiyang, Guizhou, China. The phosphorite has a Lu-Hf and Pb-Pb age of ca. 590 Ma (Barfod et al. 2002). Phosphatic stromatolites were reported in the phosphorite (Zhu and Wang 1984; Zhang et al. 1998). The other two samples (one cherty nodule embedded in dolomite and one phosphorite thin layer interlayered in black shale) are from the lower sequence of Doushantuo Formation in Yangtze Gorges area of South China, with a U-Pb age of 632 Ma (Condon et al. 2005). The Doushantuo Formation disconformably overlies Nantuo Tillite and is conformably overlain by Dengying carbonates (Xiao et al. 1998). There are abundant prokaryotic and eukaryotic microfossils and stromatolites preserved in the Doushantuo Formation (Zhu and Wang 1984; Xiao et al. 1998; Zhang et

TABLE 1.—*CONTINUED*

Samples	Age (Ma)	Flower features	Grain features		Deposition environment	Postdepositional history	Evidence of biological activities
			In flower centers	Out of flowers			
Kaiyang phosphorite	590	3–7 μm; the "petals" of apatite radial rods are much more straighter than that of the "flowers" in the above samples	50 ± 30 nm in diameter; regular shapes	50 ± 30 nm in diameter; regular shapes	in a shelf environment characterized by mixing of upwelling deep water and water masses affected by the adjacent continent weathering (Barfod et al. 2002)	Disgenesis	Stromatollite (e.g., Zhu and Wang 1984; Zhang et al. 1998).
Yangtze Gorges cherty nodule	632	–		50–150 nm; round, elliptic, polyhedron-like	peritidal to subtidal marine environments (Zhang et al. 1998; Maliva et al. 2005)	Disgenesis	prokaryotes, protists, three-dimensionally well preserved spinose acritarchs fossils, abundant unornamented spheriodal specimens of either colonial coccoid cells or individual epheroidal vesicles, and even multicellular animals in it (Zhang et al. 1998; Xiao 2004;
Yangtze Gorges phosphorite	632	3–9 μm; some of the flowers have "petals" of straight porous apatite rods while some have "petals" of radial clusters of connected apatite grains, which were coated by thin films	50–150 nm; round, elliptic, polyhedron-like	50–150 nm; round, elliptic, polyhedron-like	relatively deep intrashelf basin	Disgenesis	phosphatized fossils (e.g., Yin et al. 2004); biogenic $\delta^{34}S$ values of coexisting sulfides (Li et al. 1999)
Xiamaling black shale	1368	3–8 μm; the "petals" had straight boundaries, porous structures and rough surfaces	50–150 nm; round, elliptic	50–150 nm; round, elliptic	marine environment with high productivity of benthos (Xie et al. 2013)	Disgenesis	rich in organic matters, especially the biomakers of red algae; tetrasporangia of red algae (e.g., Zhang et al. 2007; Xie et al. 2013)
Late Archean to Neoproterozoic BIFs[a]	2460–2728	4–8 μm; the "petals" are apatite rods without porous structures or coating films	100–1000 nm; closely connected to the "petals" and appear unobviously	60 ± 35 nm in length and 30 ± 5 nm in width; rounded to elliptic; only in Dales Gorge BIF		Diagenesis and greenschist to amphibolite facies metamorphisms	

Note: Dash = none; GC-MS = gas chromatography-mass spectrometry.
[a] Samples reported in our previous studies.

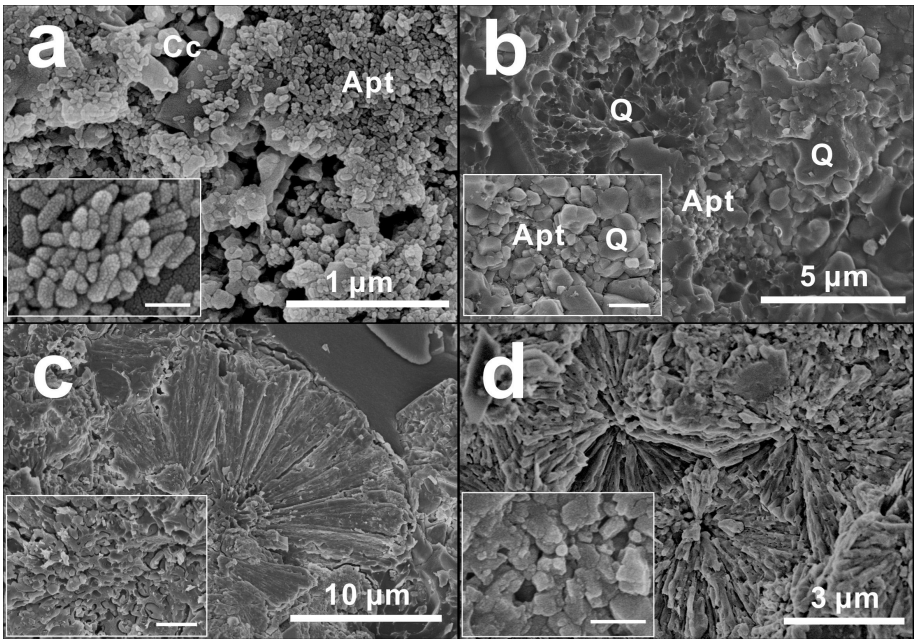

►**Figure 2.** SEM images of apatite from Lower Cambrian to Pliocene sedimentary records. (**a**) Fine-grained apatite crystals and coexisting porous calcite in the Pliocene sediments, inset is the magnified SEM image of the fine-grained apatite from the Pliocene Sediments. (**b**) Fine-grained apatite crystals and coexisting chert (quartz) from Niutitang cherty phosphorite. (**c**) Flower-like apatite in Niutitang phosphate nodules. The petals are made of apatite rods and centers are made of aggregated fine-grained apatite cemented by phosphatic matrix. Inset shows the magnified image of one flower center. (**d**) Flower-like apatite from Niutitang phosphorite. The flower petals made of apatite rods have porous structures and rough surfaces. Apt = apatite; Cc = calcite; Q = quartz. Scale bars of the insets in **a**, **b**, **c**, and **d** are: 100 nm, 1 μm, 2 μm, and 400 nm.

al. 1998; Yin et al. 2004, 2007). Globular microfossils with outer coverings and cell division were also discovered in the phosphorite layers (e.g., Xiao et al. 1998; Zhang et al. 1998).

Mesoproterozoic black shale (1368 Ma)

The Mesoproterozoic black shale was collected from the Xiamaling Formation, Xiahuayuan, North China, with a SHRIMP zircon age of 1368 Ma (Gao et al. 2008). The black shale was proposed to be an archive of early red algae because abundant legible tetrasporangia and biomarkers of red algae were identified (Zhang et al. 2007; Xie et al. 2013).

Late Archean to Paleoproterozoic banded iron formations (2728–2460 Ma)

The Late Archean to early Paleoproterozoic is a special period during which the Earth's biosphere, atmosphere and geosphere experienced profound changes (e.g., Barley et al. 2005; Campbell and Allen 2008; Bekker et al. 2010). Three BIF samples were chosen for this study (Table 1). The youngest BIF is from a drilling core (Simondium-3) of Kuruman Iron Formation, Transvaal Group, North Cape Province, South Africa, with a SHRIMP U-Pb zircon age of 2460 Ma (Pickard 2003). It has undergone low-degree metamorphisms with a peak metamorphic temperature lower than 170 °C (Miyano and Beukes 1984). The second BIF sample is from the Dales Gorge Member of Brockman Iron Formation, Hamersley Group, Western Australia, with an age of 2480 Ma (Pickard 2002). The Dales Gorge Member was subjected to metamorphic temperatures between 60 and 160 °C (Gole 1980). The oldest BIF sample in this study is from the 2728 Ma chert-jasper-magnetite facies embedded in the uppermost section of Hunter Mine Group in Abitibi, Canada, which experienced greenschist grade metamorphism (Powell et al. 1995; Mueller and Mortensen 2002).

Instruments and methods

All samples were polished to a surface with a roughness <2 μm before a thin layer was peeled off to reveal a fresh surface for immediate observation and in situ chemical analysis. Hitachi S4800 scanning electron microscope (SEM) equipped with energy-dispersive X-ray spectroscopy (EDS) was operated at low voltage (5 kV) for high-resolution morphologic characterization and high voltage (20 kV) for chemical analysis by EDS. Areas containing abundant apatite were selected for further characterization of morphology by scanning transmission electron microscope (STEM) and crystal structural analysis by selected-area electron diffraction (SAED). The selected samples were ground and loaded on copper grids with carbon-coated Formvar. The STEM-SAED analyses were conducted on FEI Tecnai G2 20 S-TWIN STEM (operated at 200 kV) equipped with SAED and EDS.

Results

Scanning electron microscopic (SEM) characterizations

Pliocene sediments (3.6 Ma Kunlun Pass sediments). In the Pliocene sediments, apatite nanocrystals with lengths of 60 ± 35 nm and widths of 35 ± 10 nm were observed (Fig. 2a). Under SEM, the apatite crystals were rounded to elliptic and tended to aggregate. No fluorine or chlorine was detected in these apatite grains by EDS. Porous carbonate (calcite) and well crystallized pyrite of ~500 nm were observed coexisting with the apatite. As apatite has extremely low abundance and small particle size, further assessment on its relation to coexisting minerals was not possible.

Niutitang cherty phosphorite (535 Ma). The Niutitang cherty phosphorite mainly consisted of quartz, clay minerals (e.g., kaolinite), and phosphate. Organic blocks were common in this cherty phosphorite. Apatite in this sample occurred as polyhedral fine grains of 100–200 nm, coexisting with euhedral quartz crystals or massive chert (Fig. 2b). Compared with the apatite nanocrystals from the Kunlun Pass sediment, apatite crystals in this sample were slightly larger and showed relatively more regular shapes.

Niutitang phosphate nodules (535 Ma). The Niutitang phos-

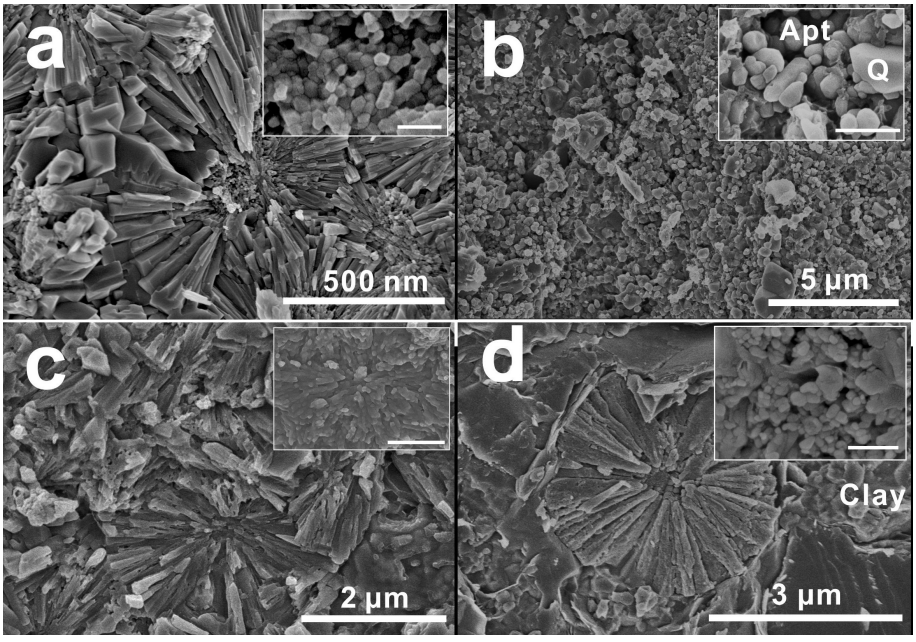

◀**FIGURE 3.** SEM images of apatite from Mesoproterozoic to Neopaleozoic sedimentary rocks. (**a**) Flower-like apatite from Kaiyang phosphorite with petals of straight boundaries and smooth surfaces, inset shows the compacted polyhedral fine-grained apatite crystals in the flower centers. (**b**) Nanoparticles of apatite from the Yangtze Gorges cherty nodule, inset is a magnified image of the fine-grained apatite coexisting with euhedral quartz. (**c**) Flower-like apatite from Yangtze Gorges phosphorite, inset shows apatite flowers of which the petals are made of connected fine-grained apatite, and the fine-grained apatite crystals coexisting them. (**d**) Apatite from Xiamaling black shale, inset shows the magnified image of fine-grained apatite in the flower centers. Scale bars of the insets in **a**, **b**, **c**, and **d** are: 250, 500, 500, and 250 nm, respectively.

phate nodules were of a few centimeters in size and embedded in black shale layers rich in organics and fossils (Steiner et al. 2001). In these nodules, apatite flower structures sized from 4 to 20 μm were observed. The flower "petals" appeared as apatite rods with inconspicuous but discernable straight boundaries and porous surfaces, while the centers were made of several 100–300 nm apatite grains with rounded to elliptic, or polyhedral shapes (Fig. 2c). The "petals" were in generally radiated from the "center" and tightly compacted together. By contrast, the fine grains in the centers were randomly oriented and cemented by phosphatic matrix. In the vicinity of flowers, the same apatite nanocrystals were also observed coexisting with quartz, clay minerals (e.g., illite), pyrite, carbonate, and occasionally barite. In the nodules, organic grains and alternating microlayers of organics and fabric apatite, which were interpreted as phosphatization products of the originally calcified organisms (Zhang et al. 1998) were frequently observed.

Niutitang phosphorite (535 Ma). Abundant apatite flowers were observed coexisting with amorphous silica, clay minerals, and gypsum in Niutitang phosphorite. Similar to previous observations (Li et al. 2013), the flowers were in the range of 3–8 μm in diameter, with "petals" composed of apatite rods and "centers" made of finer apatite crystals (Fig. 2d). The apatite rods had porous structures and rough surfaces. The ultrafine apatite crystals in the flower centers were of ~100–200 nm, similar to apatite crystals from the above-mentioned two samples from Niutitang Formation and were slightly larger than those observed in the Pliocene sediments from Kunlun Pass. These fine-grained apatite crystals in the flower centers were polyhedral and the same crystals also existed in the vicinity of apatite flowers.

Kaiyang phosphorite (590 Ma). In Kaiyang phosphorite, apatite flowers were ubiquitously observed with features similar to those in phosphate nodules or phosphorite from Niutitang Formation (Fig. 3a). They were 3–7 μm in diameter with "petals" of apatite rods and "centers" of fine-grained apatite polyhedrons (inset in Fig. 3a). Compared with the apatite flowers from Niutitang phosphatic nodules and phosphorite, the apatite rods in Kaiyang flowers showed straighter edges, more regular shapes, and smoother surfaces. The ultrafine apatite crystals in the flower centers were 50 ± 30 nm in diameter, similar to the apatite crystals in Kunlun Pass sediments. In the vicinity of flowers, abundant such fine-grained apatites were also observed coexisting with quartz and clay minerals (e.g., kaolinite).

Yangtze Gorges cherty nodule (632 Ma). The Yangtze Gorges cherty nodules were embedded in dolomite, in centimeter-size, and sometimes had a pyritic crust of ~1 mm in thickness. Apatite flowers were not observed in these nodules. However, apatite crystals with the same features to those in the centers of apatite flowers in the aforementioned samples were common. These crystals were 50–150 nm in diameter, with rounded, elliptic or polyhedral shapes (Fig. 3b). Pyrite framboids made of euhedral crystals of a few hundred nanometers were frequently found coexisting with these fine-grained apatite crystals.

Yangtze Gorges phosphorite (632 Ma). In phosphorite, apatite flowers ranging from 3 to 9 μm were observed. Some of the flowers had "petals" with straight boundaries and smooth surfaces (Fig. 3c), while the others had "petals" made of connected fine-grained apatite (inset in Fig. 3c). The apatite crystals in the flower centers (Fig. 3c) and those in the vicinity of the flowers (inset in Fig. 3c) were highly similar in terms of crystal size and morphology. They were rounded or elliptic, ranging from 50 to 150 nm. EDS analysis revealed that the apatite was fluorapatite. Pyrite framboids were also observed in the same sample. Pyrite crystals in the framboids were 1–2 μm, slightly larger than those in the pyrite framboids from the Yangtze Gorges chert nodules.

Xiamaling black shale (1368 Ma). Xiamaling black shale is an oil shale rich in organic matter (Zhang et al. 2007; Xie et al. 2013). Apatite flowers ranging from 3–8 μm were observed co-

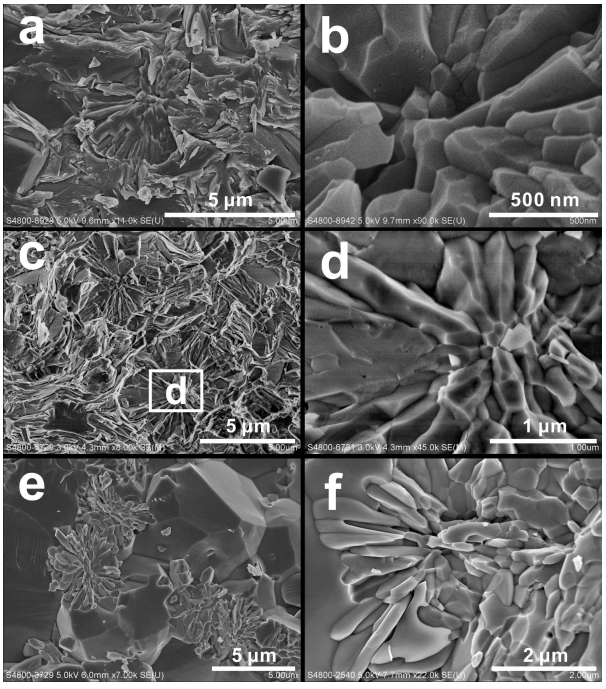

Figure 4. SEM images of apatite from Neoarchean to Paleoproterozoic BIFs. (**a**–**b**) apatite flowers from the Kuruman BIF, **b** shows the polyhedral apatite particles in the flower center. (**c**–**d**) Apatite flowers from the Dales Gorge BIF, **c** shows flow structures of the siliceous minerals around the apatite flowers, **d** shows the magnified image of the apatite grains in the flower center in **c**. (**e**–**f**) Apatite flowers from the Abitibi BIF, quartz in Abitibi BIFs shows polyhedral shapes.

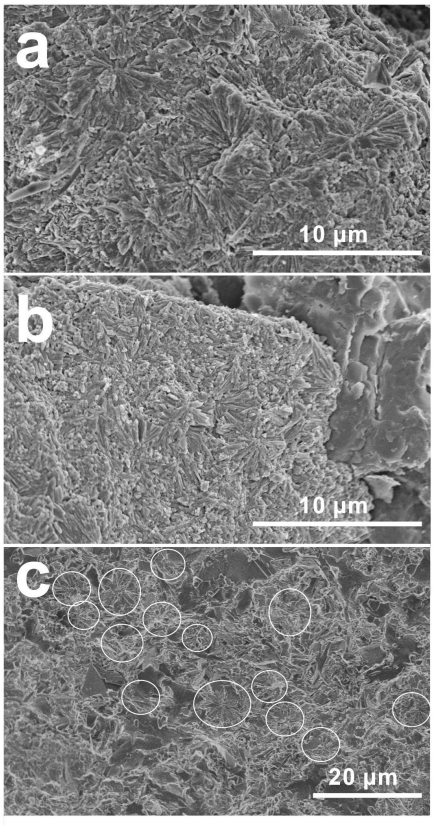

Figure 5. SEM images of the apatite flowers in larger fields of view, showing similar petrologic features of the apatite from lower Cambrian Niutitang phosphorite (**a**), Neoproterozoic Kaiyang phosphorite (**b**), and Paleoproterozoic BIF (**c**). The abundance of apatite flowers (circled areas) in BIF is much lower than that in the phosphorites.

existing with clay minerals and quartz (Fig. 3d). The apatite rods making up the "petals" showed distinct and straight boundaries, rough surfaces and porous structures. The apatite fine crystals in the centers were rounded to elliptic with diameters in the range of 50–150 nm. The same fine-grained apatite crystals were also observed coexisting with clay minerals or pyrite in the vicinity of apatite flowers (inset in Fig. 3d).

Late Archean to early Paleoproterozoic banded iron formations. In both silica- and iron-rich microbands of the three BIF samples, apatite flowers of 4 to 8 μm in diameter were observed coexisting with hematite, magnetite, or chert (Fig. 4). The flowers showed similar petrographic features as those in the phosphorites, with lower abundance (Fig. 5). The "petals" of the flowers were made of apatite rods, and the centers of the flowers were made of small apatite crystals of ~100 nm to 1 μm, which were larger than those in the apatite flowers from the Mesoproterozoic to Lower Cambrian sedimentary rocks, and showed polyhedral morphology (Fig. 4). Particularly, in BIF from Abitibi, the coexisting quartz usually appeared as polyhedrons (Fig. 4e), and the apatite nanocrystals in the centers of the apatite flowers were not conspicuous (Figs. 4e–4f).

Transmission electron microscopic (TEM) observation and selected-area electron diffraction (SAED) analysis

TEM-SAED investigations were carried out to further characterize and confirm the structures of these apatite crystals. For apatite crystals in the sediments from Pliocene Kunlun Pass and Xiamaling black shale, the SAED analyses were unsuccessful because of their low abundance and highly heterogeneous distribution. Li et al. (2013) reported that in Niutitang phosphorite, the individual apatite rods making up the flower "petals" were monocrystals as they showed well-defined regular spot arrays in their SAED patterns. Li et al. (2013) also pointed out that the apatite rods were coated by phosphatic film (apatite) made of randomly distributed ultrafine apatite crystals, as confirmed by the powder diffraction rings in the SAED pattern. High-resolution TEM characterizations in this study agreed with previous observations that the apatite rods showed homogeneous inner structures (Figs. 6a–6b) while the apatite films showed nano-sized domains of different lattice fringes (Figs. 6c–6d). In Kaiyang and Yangtze Gorges phosphorites, similar results were also obtained (Figs. 7–8). Compared with the apatite film in Niutitang phosphorite, the apatite film in Kaiyang phosphorite (Figs. 7c–7d) and Yangtze Gorges phosphorite (Figs. 8c–8d) showed relatively coarser granular textures. The lattice fringe domains of the apatite films in these two phosphorites were bigger than those in Niutitang phosphorite, indicating that the former has better crystallinity than the latter.

In Dales Gorge BIF, apatite nanocrystals highly similar to

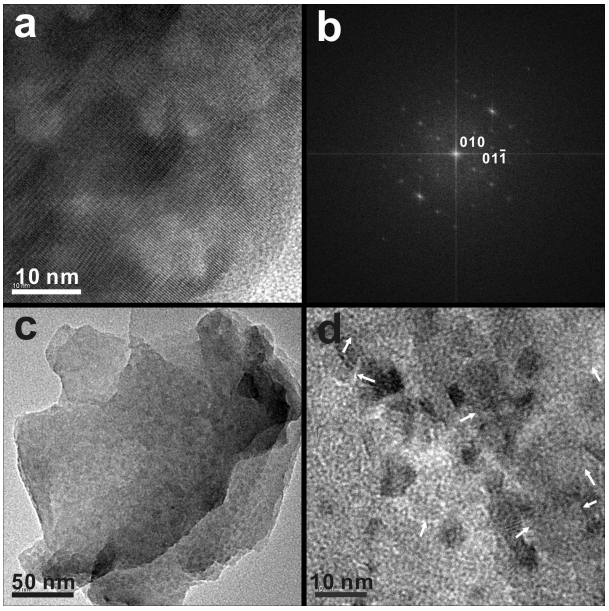

Figure 6. High-resolution TEM characterization of the apatite from Niutitang phosphorite. (**a**–**b**) lattice fringes and FFT result of the apatite rods. The lattice fringe is homogeneous in **a**, and its FFT result **b** shows well-defined spot arrays. (**c**–**d**) TEM images of phosphatic films coating the apatite rods; **d** shows 3–5 nm domains with randomly oriented lattice fringes.

those in the Kunlun Pass sediment in terms of size and shape were observed only by TEM. These nanocrystals were rounded to elliptic, with sizes of 60 ± 35 nm in length and 30 ± 5 nm in width (Fig. 9). Such apatite grains have been explained as records of phytoplanktonic cycling of phosphorus during the deposition of BIFs (Li et al. 2011).

Discussion

The apatite flowers reported here and previously (Li et al. 2013) are distinct from the large (tens to hundreds of micrometers) graphite-bearing apatite grains from the 3.8 Ga Isua Supracrustal Belt of Greenland, which were suggested to be biogenic (Mojzsis et al. 1996) but were latterly found formed in high-grade metamorphic zones (Lepland et al. 2002, 2005; Nutman and Friend 2006). In contrast, crystals described in this study are much smaller in sizes and only experienced diagenesis or low-grade metamorphisms at the most, the Kunlun Pass sediment has not even been subjected to lithification.

Despite the long geological evolution from Late Archean to Pliocene, the apatite flowers observed in 8 out of the 11 samples are highly similar in terms of morphologies, sizes and chemical compositions. Although apatite flowers are not observed in the other three samples (Pliocene Kunlun Pass sediments, Lower Cambrian Niutitang cherty phosphorite, and early Ediacaran Yangtze Gorges chert nodules), apatite nanocrystals highly similar to those in the centers of the flower structures were commonly observed in them. It is possible that the primary fabric to radial phosphate structures in the cherty phosphorite

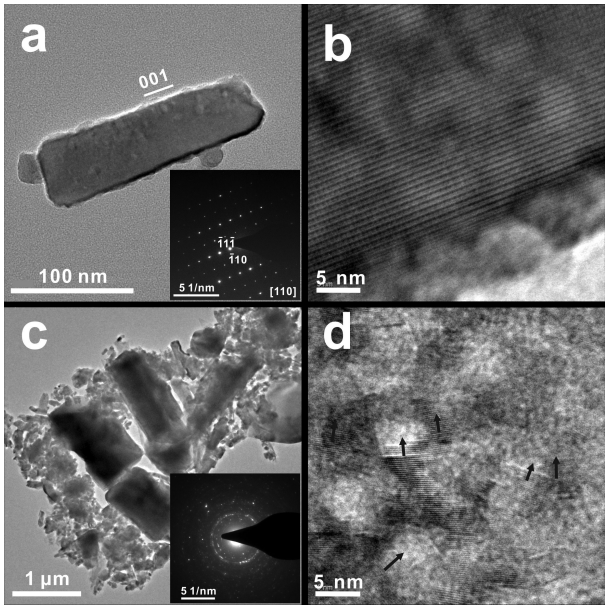

Figure 7. TEM-SAED results of apatite from Kaiyang phosphorite. (**a**) TEM image of the apatite rod and its SAED pattern (inset). (**b**) High-resolution TEM image showing homogeneous lattice fringes of the apatite rod in **a**. (**c**) TEM image of the apatite film coating the rods (the granular part surrounding the rods) and its SAED pattern (inset). The rings in the SEAD pattern indicate that the film is an aggregate of numerous ultrafine apatite particles. (**d**) High-resolution TEM image of the film in **c**, it shows randomly oriented 3–5 nm domains of lattice fringes, confirming that the film is made of numerous ultrafine apatite particles.

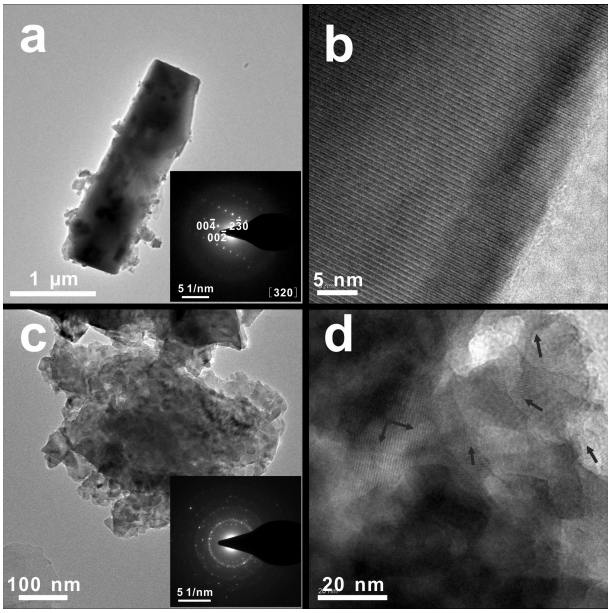

Figure 8. TEM-SAED results of apatite from Yangtze Gorges phosphorite. (**a**) TEM image of the apatite rod and its SAED pattern (inset). (**b**) High-resolution TEM image showing homogeneous lattice fringes of the apatite rod in **a**. (**c**) TEM image of the apatite film coating the rods and its SAED pattern (inset). The rings in the SEAD pattern indicate that the film is an aggregate of numerous ultrafine apatite particles. (**d**) High-resolution TEM image of the film in **c**, it shows 3–5 nm domains with randomly oriented lattice fringes, confirming that the film is made of numerous ultrafine apatite grains.

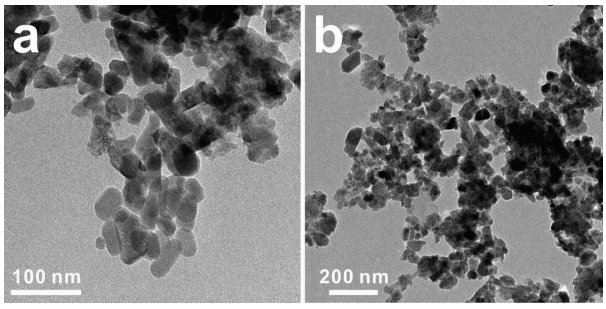

Figure 9. TEM images of the fine-grained apatite from Dales Gorge BIF.

and chert nodules have been overprinted by in situ silicification (Zhang et al. 1998). The apatite rods in flowers from the older phosphorite commonly show relatively straighter boundaries and smoother surfaces than those in the younger phosphorite, while the apatite films coating the apatite rods in the older phosphorite show coarser granular textures and better crystallinity than those in the younger phosphorite. These two parts of apatite flowers consistently show aging-induced alterations on textural and mineralogical features. With longer aging time, the nanocrystals in apatite films grew bigger, and the apatite monocrystals in "petals" developed better morphology with more regular and smoother surfaces. In BIFs, fine-grained apatite crystals in the flower centers are not conspicuous, both the porous structures and the phosphatic films even disappeared. It is probably that, due to the long diagenetic histories or low-grade metamorphisms, the fine-grained apatite in the centers and the apatite films have been integrated into the "petals". These results collectively imply that, the apatite radial flowers probably evolved from apatite nanocrystals and amorphous phosphatic gels, which either mineralized from biomass or rapidly precipitated from highly supersaturated solutions (e.g., Schulz and Schulz 2005; Goldhammer et al. 2010).

There is a consensus that organisms were involved in phosphatization processes during the deposition of phosphorite. On the one hand, the phosphorus-containing organic compounds (e.g., phospholipids) in cells could supply phosphorus for phosphate precipitation (Yang and Sun 2004; Yang et al. 2011). On the other hand, biomass of algae and animal tissue (e.g., algal cell and acritarch vesicles) could provide abundant nucleation sites for the heterogeneous nucleation of phosphate (Wilby et al. 1996; Yang and Sun 2004; Xiao and Schiffbauer 2008; Yang et al. 2011). The widely observed organic grains and organic microlayers alternating with fabric phosphatized organisms in Niutitang phosphatic nodules evidenced the biological activities during phosphatization processes. The abundant phosphatized fossils, phosphatic stromatolites, relatively high concentration of biomarkers and biogenic $\delta^{34}S$ values of coexisting sulfides in the phosphorites, from where the studied samples were collected, are also substantial lines of evidence supporting this point (Table 1 and references therein). The high similarity of the apatite nanoparticles and flowers from sedimentary records spanning ~2.7 billion-year's evolutionary history of biosphere indicates that they have experienced similar phosphatization processes (Li et al. 2013). The similarity of phosphate crystal habits allows a better understanding of phosphatization related to biomass before GOE by comparison. As BIFs formed before GOE, when the biosphere was still a microbial world (Schopf 1993; Nisbet and Sleep 2001), it can be inferred that the precipitation of apatite in BIFs was mediated by microbial activities (Nisbet and Sleep 2001; Schopf 1993, 2012). However, in the early time (before GOE), the overall oceanic primary productivity was much lower than that of the modern ocean (Papineau 2010), and the mineralization of marine phosphorus was much less, resulting in rare record of phosphorite in the sedimentary rocks.

Implications

The metabolism of microbial communities may lead to the mineralization of carbonate, iron oxides, sulfide, sulfate, and phosphorite in geological environments (e.g., Thompson and Ferris 1990; Bekker et al. 2010; Papineau 2010). The deposition of phosphorite in marine environments has been proposed to be an unequivocal part of biological cycling of phosphorus (Papineau 2010; Li et al. 2013). In this study, we present phosphate (apatite) with similar crystal habits and flower-like patterns preserved in microbial-mediated sedimentary records covering almost 2.7 billion years. Their preservation through such a deep geological time may shed some new light on searching for mineral records of possible life on Mars.

Data from Mars missions and martian meteorites suggest early Mars possessed both abundant surface waters and chemical nutrients (i.e., C, H, O, N, P, and S) required for life (e.g., Clark et al. 1976; Carr 1987; Treiman 2003; Rieder et al. 2004; Gellert et al. 2006; Bibring et al. 2006; Ming et al. 2006; Greenwood et al. 2008; Hausrath et al. 2008; Adcock et al. 2013), and there is growing evidence of past habitable environments on Mars (Williams et al. 2013; Grotzinger et al. 2014). Due to the low surface temperature (at least 50 °C lower than that on modern Earth), low atmospheric pressure (<1% of the Earth's surface pressure), up to 100 times more high-energy radiation and drastic temperature fluctuations along with wind erosion, organic substances on Mars, if any, would have been destroyed over the past three billion years (Weckwerth and Schidlowski 1995). In contrary, calcium phosphate is much more resistant to environmental changes on Mars (Weckwerth and Schidlowski 1995). In addition, the tectonic processes of Mars have been much milder than those on Earth through its whole evolutionary history (Harder and Christensen 1996; Schubert et al. 2000; Pirajno and Van Kranendonk 2005), such that the martian sediments or sedimentary rocks favor the preservation of primary geological and/or biological records (Grotzinger et al. 2011). On Earth, oxic to suboxic aquatic environments with high-primary productivity, such as the upwelling zones, favor the deposition of phosphorite (e.g., Judith and Curtis 1982; Barfod et al. 2002; Goldhammer et al. 2010). The episodic upwelling of nutrients to the photic zones of the continental shelf supports the thriving of phytoplankton that accumulates and sinks phosphorus to the sediments in the form of organic-phosphorus (Goldhammer et al. 2010). The subsequent decomposition of organics, such as the decomposition induced by sulfate-reducing and sulfide-oxidizing bacteria (e.g., Schulz and Schulz 2005; Bailey et al. 2007), releases phosphorus from the organics and

results in phosphorus supersaturation and phosphate precipitation (Goldhammer et al. 2010). Previous studies have shown that ocean once existed on Mars (e.g., Baker et al. 1991). If life has ever existed on Mars, similar phosphogenetic process should also be recorded in phosphate mineral; particularly, the radial flower patterns of a few micrometers in size are of great potential to be recognized by in situ electron microscopic observations on the fresh surface of martian sedimentary rocks.

Acknowledgment

This study was supported by General Research Fund (HKU703911P) from Research Grants Council of Hong Kong.

References cited

Adcock, C.T., Hausrath, E.M., and Forster, P.M. (2013) Readily available phosphate from minerals in early aqueous environments on Mars. Nature Geoscience, 6, 824–827.

Bailey, J.V., Joye, S.B., Kalanetra, K.M., Flood, B.E., and Corsetti, F.A. (2007) Evidence of giant sulphur bacteria in Neoproterozoic phosphorites. Nature, 445, 198–201.

Baker, V.R., Strom, R.G., Gulick, V.C., Kargel, J.S., Komatsu, G., and Kale, V.S. (1991) Ancient oceans, ice sheets and the hydrological cycle on Mars. Nature, 352, 589–594.

Barfod, G.H., Albarède, F., Knoll, A.H., Xiao, S., Télouk, P., Frei, R., and Baker, J. (2002) New Lu-Hf and Pb-Pb age constraints on the earliest animal fossils. Earth and Planetary Science Letters, 201, 203–212.

Barley, M.E., Bekker, A., and Krapez, B. (2005) Late Archean to early Paleoproterozoic global tectonics, environmental change and the rise of atmospheric oxygen. Earth and Planetary Science Letters, 238, 156–171.

Bekker, A., Slack, J.F., Planavsky, N., Krapež, B., Hofmann, A., Konhauser, K.O., and Rouxel, O.J. (2010) Iron formation: The sedimentary product of a complex interplay among mantle, tectonic, oceanic, and biospheric processes. Economic Geology, 105, 467–508.

Bibring, J-P., Langevin, Y., Mustard, J.F., Poulet, F., Arvidson, R., Gendrin, A., Gondet, B., Mangold, N., Pinet, P., Forget, F., and the OMEGA team. (2006) Global mineralogical and aqueous Mars history derived from OMEGA/Mars Express Data. Science, 312, 400–404.

Bjerrum, C.J., and Canfield, D.E. (2002) Ocean productivity before about 1.9 Gyr ago limited by phosphorus adsorption onto iron oxides. Nature, 417, 159–162.

Bowring, S.A., Grotzinger, J.P., Isachsen, C.E., Knoll, A.H., Pelechaty, S.M., and Kolosov, P. (1993) Calibrating rates of Early Cambrian evolution. Science, 261, 1293–1298.

Brasier, M.D., Green, O.R., Jephcoat, A.P., Kleppe, A.K., Van Kranendonk, M.J., Lindsay, J.F., Steele, A., and Grassineau, N.V. (2002) Questioning the evidence for Earth's oldest fossils. Nature, 416, 76–81.

Brocks, J.J. (2011) Millimeter-scale concentration gradients of hydrocarbons in Archean shales: Live-oil escape or fingerprint of contamination? Geochimica et Cosmochimica Acta, 75, 3196–3213.

Brocks, J.J., Logan, G.A., Buick, R., and Summons, R.E. (1999) Archean molecular fossils and the early rise of eukaryotes. Science, 285, 1033–1036.

Butterfield, N.J. (2007) Macroevolution and macroecology through deep time. Palaeontology, 50, 41–55.

Campbell, I.H., and Allen, C.M. (2008) Formation of supercontinents linked to increases in atmospheric oxygen. Nature Geoscience, 1, 554–558.

Canfield, D.E., Poulton, S.W., and Narbonne, G.M. (2007) Late-Neoproterozoic deep-sea oxygenation and the rise of animal life. Science, 315, 92–95.

Carr, M.H. (1987) Water on Mars. Nature, 326, 30–35.

Clark, B.C., Baird, A.K., Rose, H.J. Jr., Toulmin, P., Keil, K., Castro, A.J., Kelliher, W.C., Rowe, C.D., and Evans, P.H. (1976) Inorganic analyses of Martian surface samples at the Viking landing sites. Science, 194, 1283–1288.

Condon, D., Zhu, M., Bowring, S., Wang, W., Yang, A., and Jin, Y. (2005) U-Pb Ages from the Neoproterozoic Doushantuo Formation, China. Science, 308, 95–98.

Cook, P.J., and Shergold, J.H. (1984) Phosphorus, phosphorites and skeletal evolution at the Precambrian-Cambrian boundary. Nature, 308, 231–236.

Gao, L.Z., Zhang, C.H., Shi, X.Y., Song, B., Wang, Z.Q., and Liu, Y.M. (2008) Mesoproterozoic age for Xiamaling Formation in North China Plate indicated by zircon SHRIMP dating. Chinese Science Bulletin, 53, 2665–2671.

Gellert, R., Rieder, R., Brückner, J., Clark, B.C., Dreibus, G., Klingelhöfer, G., Lugmair, G., Ming, D.W., Wänke, H., Yen, A., Zipfel, J., and Squyres, S.W. (2006) Alpha particle X-ray spectrometer (APXS): Results from Gusev Crater and calibration report. Journal of Geophysical Research, 111, E02S05.

Goldhammer, T., Bruchert, V., Ferdelman, T.G., and Zabel, M. (2010) Microbial sequestration of phosphorus in anoxic upwelling sediments. Nature Geoscience, 3, 557–561.

Gole, M.J. (1980) Mineralogy and petrology of very-low-metamorphic grade Archaean banded iron-formations, Weld Range, Western Australia. American Mineralogist, 65, 8–25.

Greenwood, J.P., Itoh, S., Sakamoto, N., Vicenzi, E.P., and Yurimoto, H. (2008) Hydrogen isotope evidence for loss of water from Mars through time. Geophysical Research Letters, 35, L05203.

Grotzinger, J., Beaty, D., Dromart, G., Gupta, S., Harris, M., Hurowitz, J., Kocurek, G., McLennan, S., Milliken, R., Ori, G.G., and Sumner, D. (2011) Mars sedimentary geology: key concepts and outstanding questions. Astrobiology, 11, 77–87.

Grotzinger, J.P., Sumner, D.Y., Kah, L.C., Stack, K., Gupta, S., Edgar, L., Rubin, D., Lewis, K., Schieber, J., Mangold, N., and others. (2014) A Habitable Fluvio-Lacustrine Environment at Yellowknife Bay, Gale Crater, Mars. Science, 343, 1–15.

Harder, H., and Christensen, U.R. (1996) A one-plume model of martian mantle convection. Nature, 380, 507–509.

Hausrath, E.M., Navarre-Sitchler, A.K., Sak, P.B., Steefel, C.I., and Brantley, S.L. (2008) Basalt weathering rates on Earth and the duration of liquid water on the plains of Gusev Crater, Mars. Geology, 36, 67–70.

Hazen, R.M., Papineau, D., Bleeker, W., Downs, R.T., Ferry, J.M., McCoy, T.J., Sverjensky, D.A., and Yang, H. (2008) Mineral evolution. American Mineralogist, 93, 1693–1720.

Hazen, R.M., Bekker, A., Bish, D.L., Bleeker, W., Downs, R.T., Farquhar, J., Ferry, J.M., Grew, E.S., Knoll, A.H., Papineau, D., and others. (2011) Needs and opportunities in mineral evolution research. American Mineralogist, 96, 953–963.

Hoffman, P.F. (1992) Did the breakout of Laurentia turn Gondwanaland inside out? Science, 252, 1409–1412.

Hoffman, P.F., Kaufman, A.J., Halverson, G.P., and Schrag, D.P. (1998) A Neoproterozoic snowball Earth. Science, 281, 1342–1346.

Horneck, G. (2000) The microbial world and the case for Mars. Planetary and Space Science, 48, 1053–1063.

Hou, X.G., Aldridge, R.J., Bergström, J., Siveter, D.J., and Feng, X.H. (2004) The Cambrian fossils of Chengjiang, China: The flowering of early animal life, 248 p. Blackwell Publishing, Bath.

Jiang, S.-Y., Yang, J.-H., Ling, H.-F., Chen, Y.-Q., Feng, H.-Z., Zhao, K.-D., and Ni, P. (2007) Extreme enrichment of polymetallic Ni-Mo-PGE-Au in Lower Cambrian black shales of South China: An Os isotope and PGE geochemical investigation. Palaeogeography, Palaeoclimatology, Palaeoecology, 254, 217–228.

Judith, T.P., and Curtis, R.L. (1982) Atmospheric circulation, upwelling, and organic-rich rocks in the Mesozoic and Cenozoic eras. Palaeogeography, Palaeoclimatology, Palaeoecology, 40, 31–66.

Lepland, A., Arrhenius, G., and Cornell, D. (2002) Apatite in early Archean Isua supracrustal rocks, southern West Greenland: Its origin, association with graphite and potential as a biomarker. Precambrian Research, 118, 221–241.

Lepland, A., Van Zuilen, M.A., Arrhenius, G., Whitehouse, M.J., and Fedo, C.M. (2005) Questioning the evidence for Earth's earliest life-Akilia revisited. Geology, 33, 77–79.

Li, R., Chen, J., Zhang, S., Lei, J., Shen, Y., and Chen, X. (1999) Spatial and temporal variations in carbon and sulfur isotopic compositions of Sinian sedimentary rocks in the Yangtze platform, South China. Precambrian Research, 97, 59–75.

Li, Y.-L., Konhauser, K.O., Cole, D.R., and Phelps, T.J. (2011) Mineral ecophysiological data provide growing evidence for microbial activity in banded-iron formations. Geology, 39, 707–710.

Li, Y.-L., Sun, S., and Chan, L.S. (2013) Phosphogenesis in the 2460 and 2728 million-year-old banded iron formations as evidence for biological cycling of phosphate in the early biosphere. Ecology and Evolution, 3, 115–125.

Maliva, R.G., Knoll, A.H., and Simonson, B.M. (2005) Secular change in the Precambrian silica cycle: Insights from chert petrology. Geological Society of America Bulletin, 117, 835–845.

Ming, D.W., Mittlefehldt, D.W., Morris, R.V., Golden, D.C., Gellert, R., Yen, A., Clark, B.C., Squyres, S.W., Farrand, W.H., Ruff, S.W., and others. (2006) Geochemical and mineralogical indicators for aqueous processes in the Columbia Hills of Gusev crater, Mars. Journal of Geophysical Research: Planets, 111, E02S12.

Miyano, T., and Beukes, N.J. (1984) Phase relations of stilpnomelane, ferri-annite and riebeckite in very low-grade metamorphosed iron-formations. Transactions of the Geological Society of South Africa, 87, 111–124.

Mojzsis, S.J., Arrhenius, G., McKeegan, K.D., Harrison, T.M., Nutman, A.P., and Friend, C.R.L. (1996) Evidence for life on Earth before 3,800 million years ago. Nature, 384, 55–59.

Morris, R.C. (1973) A pilot study of phosphorus distribution in parts of the Brockman Iron Formation, Hamersley Group, Western Australia. Western Australia Department of Mines Annual Report, 75–81.

——— (1993) Genetic modelling for banded iron-formation of the Hamersley Group, Pilbara Craton, Western Australia. Precambrian Research, 60, 243–286.

Mueller, W.U., and Mortensen, J.K. (2002) Age constraints and characteristics of subaqueous volcanic construction, the Archean Hunter Mine Group, Abitibi

greenstone belt. Precambrian Research, 115, 119–152.
Nisbet, E.G., and Sleep, N.H. (2001) The habitat and nature of early life. Nature, 409, 1083–1091.
Nutman, A.P., and Friend, C.R.L. (2006) Petrography and geochemistry of apatites in banded iron formation, Akilia, W. Greenland: Consequences for oldest life evidence. Precambrian Research, 147, 100–106.
Papineau, D. (2010) Global biogeochemical changes at both ends of the Proterozoic: Insights from phosphorites. Astrobiology, 10, 165–181.
Pecoits, E., Gingras, M.K., Barley, M.E., Kappler, A., Posth, N.R., and Konhauser, K.O. (2009) Petrography and geochemistry of the Dales Gorge banded iron formation: Paragenetic sequence, source and implications for paleo-ocean chemistry. Precambrian Research, 172, 163–187.
Pickard, A.L. (2002) SHRIMP U-Pb zircon ages of tuffaceous mudrocks in the Brockman iron formation of the Hamersley Range, Western Australia. Australian Journal of Earth Sciences, 49, 491–507.
——— (2003) SHRIMP U-Pb zircon ages for the Palaeoproterozoic Kuruman Iron Formation, Northern Cape Province, South Africa: evidence for simultaneous BIF deposition on Kaapvaal and Pilbara Cratons. Precambrian Research, 125, 275–315.
Pirajno, F., and Van Kranendonk, M.J. (2005) Review of hydrothermal processes and systems on Earth and implications for Martian analogues. Australian Journal of Earth Sciences, 52, 329–351.
Powell, W.G., Carmichael, D.M., and Hodgson, C.J. (1995) Conditions and timing of metamorphism in the southern Abitibi greenstone belt, Quebec. Canadian Journal of Earth Sciences, 32, 787–805.
Rasmussen, B., Fletcher, I.R., Brocks, J.J., and Kilburn, M.R. (2008) Reassessing the first appearance of eukaryotes and cyanobacteria. Nature, 455, 1101–1104.
Rieder, R., Gellert, R., Anderson, R.C., Brückner, J., Clark, B.C., Dreibus, G., Economou, T., Klingelhöfer, G., Lugmair, G., Ming, D.W., and others. (2004) Chemistry of rocks and soils at Meridiani Planum from the Alpha Particle X-ray Spectrometer. Science, 306, 1746–1749.
Rothschild, L.J. (1990) Earth analogs for Martian life. Microbes in evaporites, a new model system for life on Mars. ICARUS, 88, 246–260.
Schopf, J.W. (1993) Microfossils of the early Archean Apex chert: New evidence of the antiquity of life. Science, 260, 640–646.
——— (2012) The fossil record of cyanobacteria. In B.A. Whitton, Ed., Ecology of Cyanobacteria II, p. 15–36. Springer Netherlands.
Schubert, G., Russell, C.T., and Moore, W.B. (2000) Geophysics: Timing of the Martian dynamo. Nature, 408, 666–667.
Schulz, H.N., and Schulz, H.D. (2005) Large sulfur bacteria and the formation of phosphorite. Science, 307, 416–418.
Sleep, N.H. (2010) The Hadean-Archaean environment. Cold spring harbor perspectives in biology, 2, 1–15.
Song, C., Gao, D., Fang, X., Cui, Z., Li, J., Yang, S., Jin, H., Douglas, B., and Kirschvink, J.L. (2005) Late Cenozoic high-resolution magnetostratigraphy in the Kunlun Pass Basin and its implications for the uplift of the northern Tibetan Plateau. Chinese Science Bulletin, 50, 1912–1922.
Steiner, M., Wallis, E., Erdtmann, B-D., Zhao, Y., and Yang, R. (2001) Submarine-hydrothermal exhalative ore layers in black shales from South China and associated fossils—Insights into a Lower Cambrian facies and bio-evolution. Palaeogeography, Palaeoclimatology, Palaeoecology, 169, 165–191.
Steiner, M., Zhu, M.-Y., Zhao, Y.-L., and Erdtmann, B.D. (2005) Lower Cambrian Burgess Shale-type fossil associations of South China. Palaeogeography, Palaeoclimatology, Palaeoecology, 220, 129–152.
Thompson, J.B., and Ferris, F.G. (1990) Cyanobacterial precipitation of gypsum, calcite, and magnesite from natural alkaline lake water. Geology, 18, 995–998.
Treiman, A.H. (2003) Chemical compositions of martian basalts (shergottites): Some inferences on basalt formation, mantle metasomatism, and differentiation in Mars. Meteoritics and Planetary Science, 38, 1849–1864.
Trendall, A.F., and Blockley, J.G. (1970) The iron formations of the Precambrian Hamersley Group, Western Australia. Geological Survey of Western Australia. Bulletin, 119, 1–365.
Unrug, R. (1997) Rodinia to Gondwana: The geodynamic map of Gondwana supercontinent assembly. GSA Today, 7, 1–6.
Van Zuilen, M.A., Lepland, A., and Arrhenius, G. (2002) Reassessing the evidence for the earliest traces of life. Nature, 418, 627–630.
Walter, M.R., and Des Marais, D.J. (1993) Preservation of biological information in thermal spring deposits: Developing a strategy for the search for fossil life on Mars. ICARUS, 101, 129–143.
Wang, Y., Wang, X., Xu, Y., Zhang, C., Li, Q., Tseng, Z.J., Takeuchi, G., and Deng, T. (2008) Stable isotopes in fossil mammals, fish and shells from Kunlun Pass Basin, Tibetan Plateau: Paleo-climatic and paleo-elevation implications. Earth and Planetary Science Letters, 270, 73–85.
Weckwerth, G., and Schidlowski, M. (1995) Phosphorus as a potential guide in the search for extinct life on Mars. Advances in Space Research, 15, 185–191.
Wilby, P.R., Briggs, D.E.G., Bernier, P., and Gaillard, C. (1996) Role of microbial mats in the fossilization of soft tissues. Geology, 24, 787–790.
Williams, R., Dietrich, W., Grotzinger, J., Gupta, S., Malin, M., Palucis, M., Rubin, D., Stack, K., Sumner, D., and Yingst, R. (2013) Curiosity's mastcam images reveal conglomerate outcrops with water-transported pebbles. LPI Contributions, 1719, 1617.
Xiao, S.H. (2004) New multicellular algal fossils and acriratchs in Doushantuo chert nodules. Journal of Paleontology, 78, 393–401.
Xiao, S., and Knoll, A.H. (2000) Phosphatized animal embryos from Neoproterozoic Doushantuo Formationat Weng'an, Guizhou, South China. Journal of Paleontology, 74, 767–788.
Xiao, S., and Schiffbauer, J. (2008) Microfossil phosphatization and its strobiological implications. In J. Seckbach and M. Walsh, Eds., From Fossils to Astrobiology, 89–117. Springer, Netherlands.
Xiao, S., Zhang, Y., and Knoll, A.H. (1998) Three-dimensional preservation of algae and animal embryos in a Neoproterozoic phosphorite. Nature, 391, 553–558.
Xie, L.J., Sun, Y.G., Yang, Z.W., Chen, J.P., Jiang, A.Z., Zhang, Y.D., and Deng, C.P. (2013) Evaluation of hydrocarbon generation of the Xiamaling Formation shale in Zhangjiakou and its significance to the petroleum geology in North China. Science China Earth Sciences, 56, 444–452.
Yang, H., and Sun, H.J. (2004) Crystal structure of a new phosphate compound, $Mg_2KNa(PO_4)_2 \cdot 14H_2O$. Journal of Solid State Chemistry, 177, 2991–2997.
Yang, H., Sun, H.J., and Downs, R.T. (2011) Hazenite, $KNaMg_2(PO_4)_2 \cdot 14H_2O$, a new biologically related phosphate mineral, from Mono Lake, California, U.S.A. American Mineralogist, 96, 675–681.
Yin, C., Bengtson, S., and Zhao, Y. (2004) Silicified and phosphatized *Tianzhushania*, spheroidal microfossils of possible animal origin from the Neoproterozoic of South China. Acta Palaeontologica Polonica, 49, 1–12.
Yin, L., Zhu, M., Knoll, A.H., Yuan, X., Zhang, J., and Hu, J. (2007) Doushantuo embryos preserved inside diapause egg cysts. Nature, 446, 661–663.
Zhang, Y., Yin, L., Xiao, S., and Knoll, A.H. (1998) Permineralized fossils from the terminal Proterozoic Doushantuo Formation, South China. The Paleontological Society (Memoir 50), 72, 1–52.
Zhang, S.C., Zhang, B.M., Bian, L.Z., Jin, Z.J., Wang, D.R., and Chen, J.F. (2007) The Xiamaling oil shale accumulated by Rhodophyta over 800 Ma Ago. Science China Earth Sciences, 50, 527–535.
Zhang, X.-L., Liu, W., and Zhao, Y.-L. (2008) Cambrian Burgess-type Lagerstätten in South China: Distribution and significance. Gondwana Research, 14, 255–262.
Zhu, S.X., and Wang, Y.G. (1984) Phosphatic stromatolites in Kaiyang phosphorite deposits, Guizhou, China, p. 153–164. In Proceedings of the 5th International symposium on Phosphate. Geological Publishing House, Beijing.

Manuscript received November 3, 2013
Manuscript accepted April 24, 2014
Manuscript handled by Janice Bishop